# Challenges in Integration of MMC STATCOM with Battery Energy Storage for Wind Power Plants

Sanjay Chaudhary
*Dept of Energy Technology*
*Aalborg University*
Denmark

Remus Teodorescu
*Dept of Energy Technology*
*Aalborg University*
Denmark

Łukasz Kocewiak
*Ørsted Offshore Wind*
Denmark

Philip Johnson
*Ørsted Offshore Wind*
United Kingdom
PHIJO@orsted.co.uk

Cathy Yao Chen
*Corporate Research*
*ABB AB*
Sweden
cathy-yao.chen@se.abb.com

Bertil Berggren
*Corporate Research*
*ABB AB*
Sweden

Lennart Harnefors
*Corporate Research*
*ABB AB*
Sweden

***Abstract*—As the conventional power plants are being replaced by renewable energy sources like wind and solar, large power plants based upon the renewable energy sources are expected to provide ancillary services and functionalities like voltage and frequency regulation, and to mitigate the variability of power supply. Thus, there is a need for the control of both active and reactive power generation from the plant. Wind power plants have limited controllability of active power due to their dependency upon the instantaneous wind conditions; while the reactive power should be locally compensated at the Point of Connection (PoC). This paper describes the application of a modular multilevel converter (MMC) static compensator (STATCOM) with Battery Energy Storage System (BESS) as an integrated solution to these requirements. Simulation results demonstrate the inertial as well as fast droop response for frequency control, while the voltage regulation is relatively slow process.**

***Keywords— battery energy storage system (BESS), modular multilevel converter (MMC), point of connection (PoC).***

## I. Introduction

There has been tremendous growth in the installation of wind power plants (WPPs) worldwide. According to World Wind Energy Association (WWEA), the total installed wind capacity reached 597GW by the end of 2018, out of which 50.1 GW was added in 2018 itself [1]. WPPs have increased power and capacity at both the turbine level as well as the plant level. Nowadays there are several large WPP bigger than a few hundred megawatts. Recently, Hornsea One offshore WPP of 1200 MW size has been developed [2]. Several other WPPs bigger than 1000 MW, like Hornsea Two and Three, Dogger Bank in the UK, Ocean Wind project in the USA, and Changhua in Taiwan, are under different stages of development. Consequently, conventional power plants are being replaced by renewable energy sources, thereby, leading to the loss of fully controllable and dispatchable power sources with inherent inertia, and reliable capability for frequency and voltage support to the power system [3], [4]. Moreover, the offshore WPP layout entails long high voltage (HV) and medium voltage (MV) cable connections, a large number of reactors to absorb the excess var generated by the cables, harmonic filters and usually three transformer stages between the wind turbine (WT) units spread over a large area and the point of connection (PoC) in the onshore grid [2], [5].

Due to long distance separation of the WPP from the onshore grid, the voltage control at the PoC onshore is challenging. A static synchronous compensator (STATCOM) will be needed to provide voltage regulation and enable fault ride through capability by injecting reactive currents during low voltage faults in the grid [6]. Similarly, some sort of energy storage is needed if the WPP has to respond to frequency deviations. In such a case, a battery energy storage system (BESS) is an option [7]. Since the battery units are available only at low voltage levels integration of the battery and the STATCOM in a single converter unit is challenging. Reference [8] describes the use of energy storage in super-capacitors to provide power intensive frequency support for short periods. While this can be acceptable for decreasing the rate of change of frequency (ROCOF), the primary frequency response is limited to short periods due to small energy storage capacity of the supercapacitors. This paper describes a STATCOM with BESS and then demonstrates some of its application examples on a test WPP model.

This paper is organized as follows. The MMC topology for the STATCOM with BESS and the different control structures are briefly described in Section II. It is followed by the simulation results for the demonstration of inertial and droop frequency control response against frequency deviations and voltage regulation in a test model of wind power plant. The final conclusions are provided in Section V.

## II. DSFB-CES Topology

Several different topologies of the MMC using star or delta connection of full-bridge, half-bridge and hybrid converters for the MMC were analysed. Likewise, for the energy storage units the centralized and distributed energy storage options were evaluated. Finally, double star connection of full-bridge cells (DSFB) with centralized energy storage (CES) was selected as the optimal topology (Fig. 1). It provided lower losses, increased utilization of the semi-conductor devices, and lower dc link voltage for the connection of Li-ion battery units in the CES.

This work has been funded by Innovation Fund - Grand Solutions, Denmark.

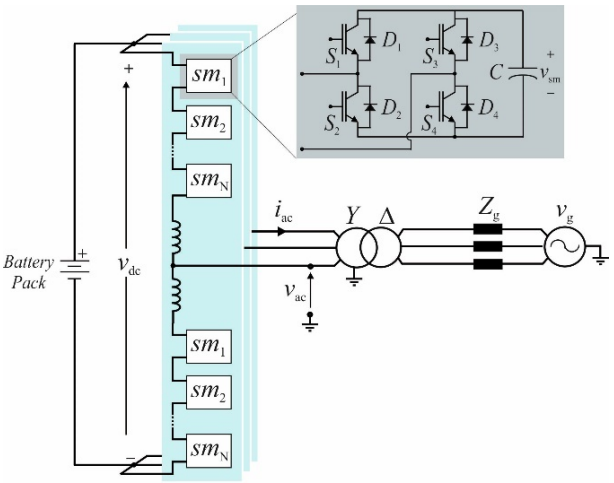


**Fig. 1. Double star full-bridge (DSFB) MMC with centralized energy storage (CES).**

### A. DSFB-CES ratings

In this work a 100 Mvar STATCOM unit has been considered with simultaneous active power of 50 MW from the dc battery units. Therefore, the power converter has to be rated for 112 MVA. It is connected to the 220-kV grid through a 33/220-kV step-up transformer. Other ratings are given in Table I. There are 19 full-bridge cells (also referred to as sub-modules) in each of the six arms of the converter. Use of full-bridge cells allows the generation of negative voltages from cells and hence, the minimum required sum voltage of each arm is 42.4 kV under nominal grid conditions of 1 pu voltage and considering 8% reactance in the arm-reactors and 12% leakage reactance of the transformer. Some margin has to be provided to account for the variation of the dc link voltage as the battery voltage varies with its state of charge.

Centralized energy storage was preferred over the distributed battery units, as described in [9], as this allows the separation of the battery units from the converter units. Thus, the battery racks can be stored in a temperature-controlled housing away from the higher operating temperature of the converter. However, this complicates the protection of the battery units against dc short circuit faults. Therefore, a lower voltage of the battery was selected to utilize the dc circuit breakers, available at lower dc voltage levels.

TABLE I. TABLE I. NOMINAL RATING OF THE MMC STATCOM WITH BESS

| | | |
|---|---|---|
| DC link voltage | 20 | kV |
| AC voltage | 33 | kV |
| Active power | 50 | MW |
| Reactive power | 100 | Mvar |
| Number of sub-modules | 20 | |
| Sub-module voltage | 2.25 | kV |
| Sub-module capacitance | 16.4 | mF |
| Arm inductance | 3.1 | mH |

### B. Control of DSFB-CES

The MMC control can be divided into two levels: (i) Converter level control and (ii) System level control.

*1) Converter level control*

The converter level control aims at controlling and balancing the cell voltages at around the nominal levels of 2.25 kV. This is achieved by controlling the circulating current in the converter arms. The arm voltages to be inserted by each of the six arms of the converter is determined on the basis of the ac- and dc- terminal voltages of the converter, cell voltages, and required circulating current and output current. Once the arm voltages are determined, the sort and select modulation is employed to determine the cells to be bypassed or inserted in positive or negative mode.

*2) System level control*

The system level control determines the response of the converter to the grid. In this work, the active and reactive power of the converter are controlled in order to support the grid frequency and voltage respectively. A phase locked loop is used to determine the phase angle of the grid. The frequency and voltage regulation loops determine the required active and reactive power references. The error in active and reactive power references is applied to a proportional-integral controller to generate the current references in the synchronously rotating reference frame. The inner current control loop along with the feed-forward voltage and the decoupling terms determine the output voltage to be generated by the converter. Finally, it is applied to the converter level control described before.

### C. Ancillary services for grid support

The selected ancillary services are synthetic inertia, primary frequency control, voltage support and reactive current injection during under-voltage ride through conditions. Active and reactive power control loops are implemented in the system level control as described earlier.

*1) Synthetic inertia emulation*

Unlike the synchronous generator, this converter does not possess inherent inertia. Rather it is decupled from the grid frequency by the converter controlled in the grid following mode. Hence, the rate of change of frequency (ROCOF) is approximated by passing the measured frequency, as obtained from the phase locked loop (PLL), through a washout filter as shown in Fig. 2. The resultant signal is then multiplied by a gain to reflect the inertial response, $P_{ir}$, given by,

$$P_{ir}(s) = K_{ir}\frac{s}{s+\alpha}\omega_m(s). \quad (1)$$

Here $K_{ir}$, $\alpha$ and $\omega_m$ are the gain of the inertial response, corner frequency of the washout filter and measured angular frequency of the grid. The power commanded by the inertial response is then applied to the power reference of the active power controller.

*2) Droop frequency control*

The power command, $\Delta P_{dr}$, corresponding to the deviation of the measured grid frequency from the nominal frequency, $\omega_0$, is generated using the droop equation given below,

$$\Delta P_{dr} = K_{dr}(\omega_0 - \omega_m). \quad (2)$$

Here $K_{dr}$ is the gain of the power frequency droop characteristic. The resultant active power is then added to the active power reference as shown in Fig. 2.

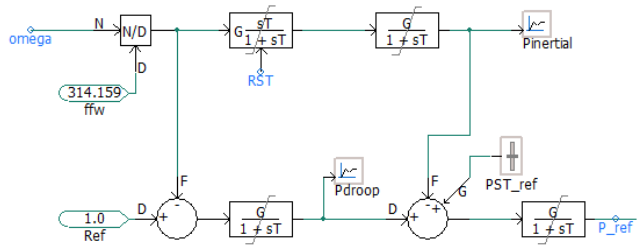


**Fig. 2. Synthetic inertia and droop frequency controller.**

*3) Voltage support*

The reactive power reference to the STATCOM is augmented by an input, $\Delta Q_{st}$, for grid voltage support in response to the voltage deviation from the reference as given by,

$$\Delta Q_{st}(s) = \frac{sT_iK_p+1}{sT_i(K_{vd}K_p+1)+K_{vd}}\Delta V_g(s) \qquad (3)$$

where $K_p$ and $T_i$ are the proportional gain and integral time constant of the PI controller for voltage support, and $K_{vd}$ is a droop parameter for voltage support as shown in Fig. 3.

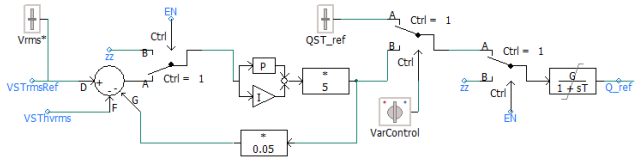


**Fig. 3. Controller for grid voltage support by the STATCOM.**

*4) Reactive current injection during low voltage fault ride through (LVRT)*

This control is activated when the voltage deviation exceeds the dead-band of ±10%. The positive sequence reactive current reference is generated in proportion to the voltage deviation beyond the dead-band and applied to the current controller. It is not implemented here for the sake of simplicity.

## III. Simulation of Ancillary Services in the Test WPP Model

A test WPP model has been created on the basis of Hornsea Two WPP in the UK. The WPP comprises of 3 groups of 55x8-MW WT units each. Accordingly, all the electrical infrastructure has been installed in triplicate to maintain the plant symmetry. In this work, however, only a third of the plant has been modelled and hence, it represents a 440 MW offshore wind power plant as shown in Fig. 4.

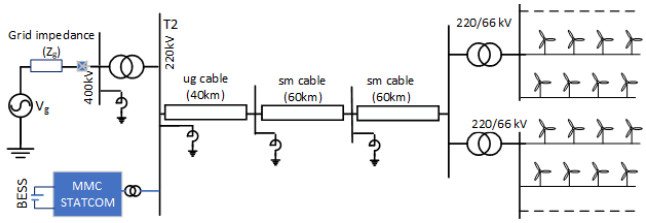


**Fig. 4. Network model of a large offshore wind power plant.**

The onshore grid is represented by a Thevenin equivalent voltage source of 6600 MVA short circuit capacity. The WPP output is ramped up from 0 MW to 440 MW within 3s of simulation. The reactors on the bus T2 can be switched on/off manually. The MMC STATCOM is connected to the 220-kV bus through a 33/220-kV transformer. The MMC model was separately simulated, and in this work an average voltage source model of the MMC has been used.

The voltage magnitude and frequency of the voltage source can be modified externally to simulate the step changes in voltage magnitude and frequency. Two cases, one for step change in frequency and another for step change in terminal voltage, have been simulated and the response from the MMC STATCOM with BESS unit has been described below. The STATCOM acts like the interfacing converter between the BESS and the grid for the exchange of active power.

### A. Step change in frequency

Step changes of 1% (i.e. 0.5 Hz) are applied to the frequency of the voltage source representing the grid. Since the system inertia is not modelled here, the grid frequency changes instantly as shown in Fig. 5a. The STATCOM with BESS responds to the frequency changes by providing the inertial response as well as the primary frequency response defined by the 10% power frequency droop which implies that the BESS output will increase by 100% for 10% drop in frequency. In this case the frequency increases by 1% (0.5 Hz) at 5.5s and the droop frequency response provides −5.0 MW within 150ms. Likewise, when the frequency decreases by 1% above nominal at 6.5s, the droop frequency response provides 5 MW in steady state.

The ROCOF for synthetic inertia emulation is obtained using a wash-out filter with a time constant of 31.83s which corresponds to a low pass filter of 5-Hz applied to the derivative block (Fig. 2). An inertia constant of 1.5s provides a reference of −16.7 MW within 54ms. Higher values could not be used to avoid the amplification of the noise from the wash-out filter. Since a step change is applied to the grid voltage source, the actual rate of change of frequency would be infinite. The computed value of ROCOF from the frequency estimated by the PLL at 5.5s and 5.53s indicate a ROCOF of 16.7 Hz/sec. The output of the wash-out filter gives a maximum ROCOF of 11.57 Hz/s at 5.51s However, the inertial response is not very high as there is an additional low pass filter with a time constant of 30ms in the gain block for inertia constant. Even afterwards, another low pass filter with a 20-ms time constant is applied to filter the reference power applied to the converter.

In fact, the droop frequency response and the inertial response appear simultaneously in the beginning. The only difference is that the component of the reference from the inertial response changes rapidly as shown in Fig. 5d since it acts on the ROCOF. The inertial response reaches a peak 16.9 MW within 41ms and then falls down to 0 within 180ms as the ROCOF tends to stabilize (Fig. 5d). The droop frequency response, on the other hand, rises slowly to reach −5.0 MW in 154ms as shown in Fig. 5c.

The actual active power reference reaches a minimum of −17.5 MW after 29ms when the measured output power at the STATCOM terminals is minimum at −16.6 MW. At this instant the reference component from the inertia emulation −13.6 MW and the component from the droop frequency controller is −3.9 MW.

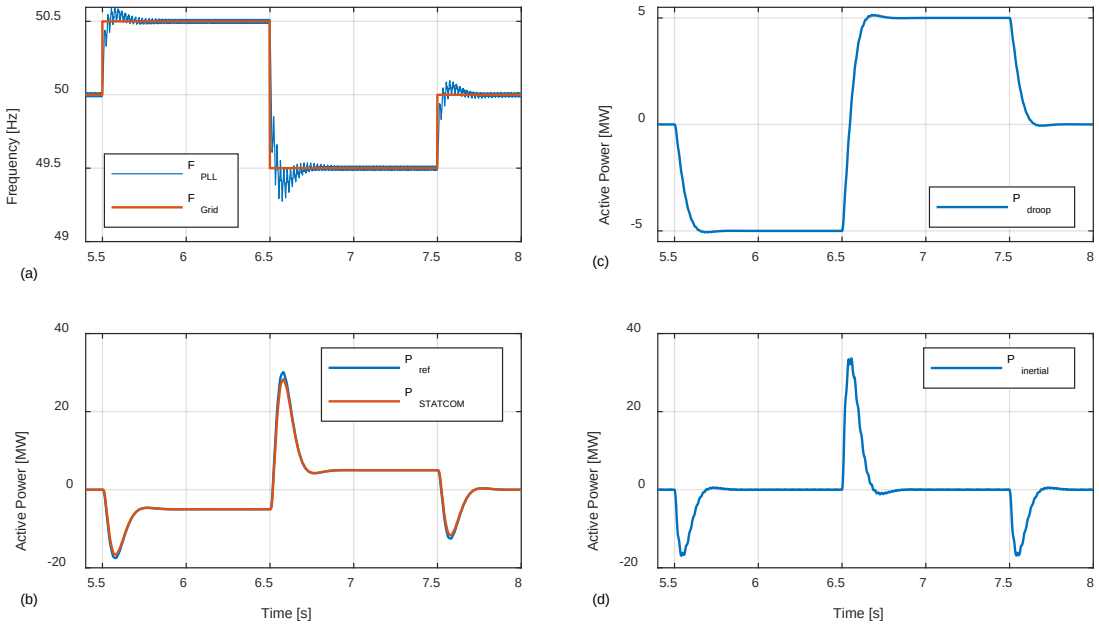


**Fig. 5. Frequency response by STATCOM with BESS: (a) Actual ($F_{Grid}$) and measured ($F_{PLL}$) grid frequency. (b) Active power injection- reference ($P_{ref}$) and injected ($P_{STATCOM}$). (c) Active power reference for frequency droop response. (d) Active power reference for inertial power reference.**

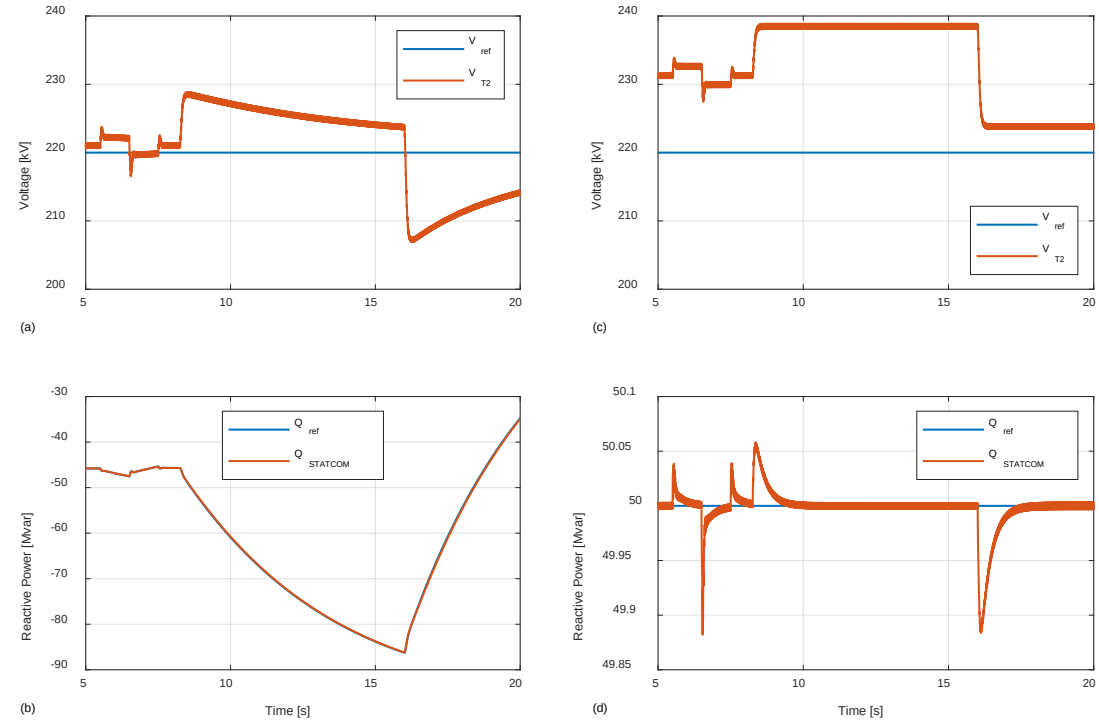


**Fig. 6. Voltage support by STATCOM: (a) Terminal voltage at T2 with voltage support from STATCOM. (b) Reactive power reference ($Q_{ref}$) and injected reactive power from STATCOM for voltage support. (c) Terminal voltage at T2 without any voltage support from STATCOM. (d) Constant reactive power reference ($Q_{ref}$) of 50 Mvar and injected reactive power from STATCOM.**

In the next event at 6.5s, the grid frequency changes from 50.5 Hz to 49.5 Hz, i.e. a step change of 2% is applied. The corresponding ROCOF at the output of the washout filter is −23.1 Hz/s after 12ms and the maximum inertial response is 33.4 MW after 140ms. The maximum active power reference for frequency support functionality is achieved after 79ms when the inertial emulation contributes 27.6 MW and the droop frequency controller contributes 2.8 MW. The component from the droop frequency response reaches 5 MW after 150ms.

### *B. Step change in terminal voltage*

The step change in voltage is achieved by first increasing the 400-kV grid voltage to 410kV at 8.25s. The voltage at the 220-kV terminals (referred here as T2) of the grid transformer rises to 228 kV at 8.4s. The 100 Mvar STATCOM is connected to regulate the grid voltage with a 10% voltage regulation droop at T2. The reactive power absorbed by the STATCOM starts increasing, and it reaches 86 Mvar at 16s and the voltage is reduced to 223.8 kV level. In another case, when the STATCOM was on constant reactive power control mode, absorbing a constant var of 50 Mvar, the grid voltage at T2 increased from 231 kV to 238 kV as a result of the step change in the grid voltage.

The voltage regulation function is a slow function and hence the steady-state was not attained by the instant when the grid voltage was reduced to 390 kV by an external step change input. The var absorbed by the STATCOM starts decreasing as the grid voltage falls below the reference of 220 kV at T2. The var absorption decreases to 35 Mvar in 4 s and is still decreasing as shown in Fig 6(b). When there is constant var absorption of −50 Mvar, the voltage at T2 drops from 238.5 kV to 224 kV. This shows the voltage regulation capability of the STATCOM. Dynamics of voltage regulation appears to be slow as steady-state was not attained in the simulated time period of around 9s after the step change in voltage.

## IV. Conclusions

A high-voltage STATCOM with integrated BESS component has been proposed and its application in a WPP has been demonstrated through simulation.

A DSHB-CES topology of MMC has been selected for the implementation of the STATCOM and BESS systems. Afterwards, its application to provide synthetic inertia and droop regulation for frequency control by controlling the active power exchanged from the BESS system has been shown. In the present implementation, using grid following converters, the inertial response depends upon the estimation of rate of change of frequency using a wash-out filter. Additional filters are used to suppress the high frequency noise component.

Similarly, the 10% droop has been implemented in the STATCOM for voltage regulation at a 220-kV bus on the onshore grid. The dynamics of voltage regulation appears to be much slower in comparison to the frequency controller. The relative difference between these might also be attributed to the way the two responses are evaluated. While the frequency response is measured in terms of the power injected into the grid with very large inertia (infinite in this work) in comparison to the BESS size, the voltage response is dependent upon the local bus voltage dynamics. Hence, the voltage regulation control loop is deliberately kept slower.

## Acknowledgment

The authors acknowledge the comments and inputs from Daniela Pagnani, Ørsted Offshore Wind, Denmark.

## References

[1] World Wind Energy Association. (2019) Wind Power Capacity Worldwide Reaches 597 GW, 50,1 GW added in 2018. [Online]. Available:https://wwindea.org/blog/2019/02/25/wind-power-capacity-worldwide-reaches-600-gw-539-gw-added-in-2018/

[2] J. Hjerrild, S. Sahukari, M. Juamperez, Ł. H. Kocewiak, M. A. Vilhelmsen, J. Okholm, M. Zouraraki, T. Kvarts, "Hornsea Projects One and Two – Design and Execution of the Grid Connection for the World's Largest Offshore Wind Farms," Cigre Symposium Aalborg, Denmark, 4-7 June 2019.

[3] F. Blaabjerg, Y. Yang, D. Yan g and X. Wang, "Distributed Power-Generation Systems and Protection," in Proceedings of the IEEE, vol. 105, no. 7, pp. 1311-1331, July 2017.

[4] High Penetration of Power Electronic Interfaced Power Sources (HPoPEIPS), ENTSO-E Guidance document for national implementation for network codes on grid connection, 29 March 2017.

[5] M. Lehmann, M. Pieschel, Ł. H. Kocewiak, M. Juamperez, S. Sahukari, K. Kabel, "Active Filtering with Large-Scale STATCOM for the Integration of Offshore Wind Power," in Proc. The 17th International Workshop on Large-Scale Integration of Wind Power into Power Systems as well as Transmission Networks for Offshore Wind Farms, Energynautics GmbH, 17-19 October 2018, Stockholm, Sweden.

[6] Pertl, M., Weckesser, J. T. G., Rezkalla, M. M. N., & Marinelli, M. (2017). Transient stability improvement: a review and comparison of conventional and renewable-based techniques for preventive and emergency control. Electrical Engineering. https://doi.org/10.1007/s00202-017-0648-6

[7] L. Wu, W. Gao, Z. Cui and X. Kou, "A Novel Frequency Regulation Strategy with the Application of Energy Storage System for Large Scale Wind Power Integration," 2015 Seventh Annual IEEE Green Technologies Conference, New Orleans, LA, 2015, pp. 221-226. doi: 10.1109/GREENTECH.2015.34

[8] E. Spahic, C. P. Susai Sakkanna Reddy, M. Pieschel and R. Alvarez, "Multilevel STATCOM with power intensive energy storage for dynamic grid stability - frequency and voltage support," 2015 IEEE Electrical Power and Energy Conference (EPEC), London, ON, 2015, pp. 73-80. doi: 10.1109/EPEC.2015.7379930

[9] M. Vasiladiotis and A. Rufer, "Analysis and control of modular multilevel converters with integrated battery energy storage," IEEE Transactions on Power Electronics, vol. 30, pp. 163–175, Jan 2015.